Korean J. Chem. Eng., **30**(5), 1023-1028 (2013)
DOI: 10.1007/s11814-013-0013-z

Stability analysis of compositional convection in a mushy layer in the time-dependent solidification system

In Gook Hwang†

Department of Chemical Engineering, University of Suwon, Gyeonggi-do 445-743, Korea
(*Received 26 November 2012 • accepted 30 January 2013*)

Abstract−Instabilities of convection in a mushy layer with a permeable interface underlying a liquid layer are studied in the time-dependent solidification system in which a binary melt cooled from below. The self-similar stability equations in the liquid and mushy layers are derived by propagation theory. The onset of mushy-layer-mode convection is examined considering the variation of permeability with porosity in the mushy layer. The numerical results show that the critical Darcy-Rayleigh number defined in terms of the mean permeability increases with increasing the concentration ratio and decreases with increasing the superheat. When the concentration ratio is small, a small convective cell appears in the vicinity of the liquid-mush interface. The influences of various non-uniform permeability models on the stability of compositional convection are discussed.

Key words: Convective Instability, Solidification, Mushy Layer, Permeability Variation

INTRODUCTION

Solidification is an important process in crystal growth for the semi-conductor industry, the casting of alloys, and the fabrication of composites. In binary solidification solutal convection can occur in a mushy layer, resulting in the formation of freckles in solidified alloys [1-3]. The mushy layer is a region of solid-liquid mixed phase formed between the melt and solid layers and it is treated as a porous medium in fluid mechanics [4,5].

Fowler [6] investigated theoretically the formation of freckles and convective instability in the mushy layer. Worster [7] and Chen et al. [8] analyzed two modes of convection in steady solidification of the mushy layer: boundary-layer instability and mushy-layer instability. Their work was extended by considering the effects of inclined rotation and rocking motion [9,10]. Emms and Fowler [11] evaluated the similarity solutions of the basic equations and the onset conditions in the mushy layer using the quasi-static stability analysis. Tait and Jaupart [12] conducted experiments on the natural convection in the mushy layer using aqueous ammonium chloride solution. And various studies have been carried out on convection in the mushy layer [13-19].

In this work the onset of convection in the mushy layer during binary solidification is investigated by using propagation theory [20-26]. Propagation theory deals with the convective instability, considering the time-dependency in an approximate way and produces the self-similar stability equations in terms of a similarity variable. Hwang and Choi's [24] results of the critical thickness of the mushy layer compare well with Tait and Jaupart's [12]. In the present study the Lewis number is assumed to be zero and the effect of the thermal buoyancy force is neglected in the liquid layer. The Lewis number is defined as $Le=D/\kappa$, where D is the solute diffusivity and κ is the thermal diffusivity. When $Le\rightarrow 0$, the compositional boundary layer is ignored and the concentration field is not considered in the liquid layer, resulting in only the mushy-layer-mode convection. The mushy-layer-mode instability is analyzed using the mushy-layer thickness as a length scale. The effect of the variation of permeability with local porosity in the mushy layer on the convective instability is studied. The critical conditions obtained from various non-uniform permeability models are compared with those from the uniform permeability model.

GOVERNING EQUATIONS

Consider the solidification system shown in Fig. 1, in which a binary solution of temperature T_∞ and solute composition C_∞ is solidified time-dependently from the bottom boundary [20,25]. The position of a liquid-mush interface H(t) moves upwards in proportion to the square root of time t. The mush-solid interface is at the eutectic temperature T_E and the eutectic composition C_E. In the mushy layer

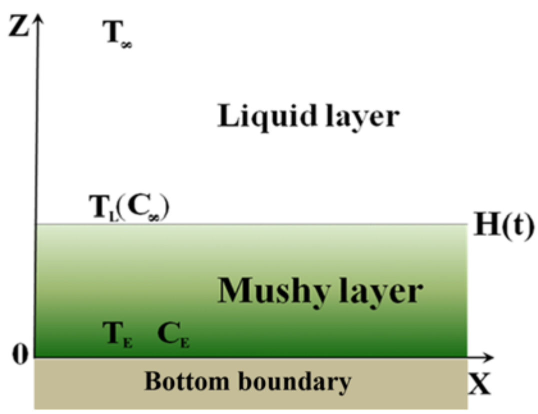

Fig. 1. A schematic diagram of the solidification system in which a binary melt is cooled from a bottom boundary. The position of a liquid-mush interface H($\propto\sqrt{t}$) moves upwards with time.

†To whom correspondence should be addressed.
E-mail: ighwang@suwon.ac.kr

thermodynamic equilibrium is maintained and the liquidus temperature T_L is given by the following liquidus relationship:

$$T_L=T_L(C_\infty)+\Gamma(C-C_\infty), \tag{1}$$

where Γ is the slope of the liquidus curve.

In the present study the permeability variation in the mushy layer is considered. The governing equations for the mushy layer are written in dimensionless form as follows:

$$\left(\frac{\partial}{\partial\tau}+\mathbf{u}_m\cdot\nabla\right)\theta_m=\nabla^2\theta_m-\mathrm{St}\frac{\partial\chi}{\partial\tau}, \tag{2}$$

$$\chi\frac{\partial c_m}{\partial\tau}+\mathbf{u}_m\cdot\nabla c_m=(\gamma-c_m)\frac{\partial\chi}{\partial\tau}, \tag{3}$$

$$\frac{\mathbf{u}_m}{\Pi(\chi)}=-\mathrm{Da}\nabla p_m+\mathrm{R}_m\theta_m\mathbf{e}_k, \tag{4}$$

$$\nabla\cdot\mathbf{u}_m=0, \tag{5}$$

where $\mathbf{u}$ denotes the velocity vector, τ is time, p is pressure, and $\mathbf{e}_k$ is the unit vector in the z-direction. The subscript 'm' represents the properties of the mushy layer. The distance has been scaled by an arbitrary length L, time by L^2/κ, velocity by κ/L, and pressure by $\mu\kappa/L^2$, where μ is the viscosity. The dimensionless permeability $\Pi(\chi)$ is a function of local liquid fraction (or porosity) χ, defined as $\Pi(\chi)=\Pi_*(\chi)/\Pi_r$, where Π_r is the reference permeability. Π_r is chosen as the mean permeability of the mushy layer $\Pi_*(\overline{\chi})$ or as its value at the liquid-mush interface $\Pi_*(1)$. In the liquid layer it is assumed that the Lewis number Le is zero and thermal buoyancy is neglected [7]. Under these simplifying assumptions the governing equations in the liquid are given by

$$\left(\frac{\partial}{\partial\tau}+\mathbf{u}\cdot\nabla\right)\theta=\nabla^2\theta, \tag{6}$$

$$\frac{1}{\mathrm{Pr}}\left(\frac{\partial}{\partial\tau}+\mathbf{u}\cdot\nabla\right)\mathbf{u}=-\nabla p+\nabla^2\mathbf{u}, \tag{7}$$

$$\nabla\cdot\mathbf{u}=0. \tag{8}$$

The dimensionless temperature and concentration are defined as

$$\theta=\frac{T-T_L(C_\infty)}{\Delta T},\ \ c=\frac{C-C_\infty}{\Delta C}, \tag{9}$$

where $\Delta T=\Gamma\Delta C=T_L(C_\infty)-T_E$, $\Delta C=C_\infty-C_E$, and $\theta_m=c_m$ in the mushy layer. The dimensionless parameter St is the Stefan number ($=\overline{L}/(C_P\Delta T)$), Pr the Prandtl number ($=\nu/\kappa$), and γ the concentration ratio ($=(C_s-C_\infty)/\Delta C$), where $\overline{L}$ is the latent heat of fusion, ν the kinematic viscosity, C_p the specific heat, and C_s the solute concentration in the solid. The Darcy-Rayleigh number R_m is defined as $R_m=g\beta_m\Delta C\Pi_r L/\kappa\nu$; where g denotes the gravity acceleration, $\beta_m(=\beta-\alpha\Gamma)$ the effective expansion coefficient, α the thermal expansion coefficient, and β the solutal expansion coefficient. The Darcy number is defined as $\mathrm{Da}=\Pi_r/L^2$.

In the basic state of no convection the governing equations are transformed in terms of a similarity variable $\zeta=z/(2\lambda\tau^{1/2})$. The dimensionless thickness of the mushy layer h (=H/L) has the relation of $h=2\lambda\tau^{1/2}$, where the phase-change rate λ is a constant. The self-similar basic equations are

(in the liquid layer)

$$\frac{d^2\theta_0}{d\zeta^2}+2\lambda^2\zeta\frac{d\theta_0}{d\zeta}=0 \qquad \text{for } \zeta>1, \tag{10}$$

(in the mushy layer)

$$\frac{d^2\theta_{m0}}{d\zeta^2}+\left[1+\mathrm{St}\frac{\gamma}{(\gamma-\theta_{m0})^2}\right]2\lambda^2\zeta\frac{d\theta_{m0}}{d\zeta}=0 \qquad \text{for } \zeta<1, \tag{11}$$

where the subscripts '0' and 'm0' represent the basic quantities of the liquid and mushy layers, respectively. The porosity in the mushy layer is $\chi_0=\gamma/(\gamma-\theta_{m0})$ with $\chi_0=1$ at $\zeta=1$. The boundary conditions are

$$\theta_0=\theta_\infty \qquad \text{for } \zeta\to\infty, \tag{12}$$

$$\theta_0=\theta_{m0}=0,\ \frac{d\theta_0}{d\zeta}=\frac{d\theta_{m0}}{d\zeta} \qquad \text{at } \zeta=1, \tag{13a,b}$$

$$\theta_{m0}=-1 \qquad \text{at } \zeta=0, \tag{14}$$

where θ_∞ ($=(T_\infty-T_L(C_\infty))/\Delta T$) represents the superheat.

STABILITY ANALYSIS

For the mushy layer with permeability variation the following disturbance equations are obtained from the governing equations under linear stability theory:

$$\frac{\partial\theta_{m1}}{\partial\tau}+\mathrm{R}_m w_{m1}\frac{\partial\theta_{m0}}{\partial z}=\nabla^2\theta_{m1}-\mathrm{St}\frac{\partial\chi_1}{\partial\tau}, \tag{15}$$

$$\chi_1\frac{\partial\theta_{m0}}{\partial\tau}+\chi_0\frac{\partial\theta_{m1}}{\partial\tau}+\mathrm{R}_m w_{m1}\frac{\partial\theta_{m0}}{\partial z}=(\gamma-\theta_{m0})\frac{\partial\chi_1}{\partial\tau}-\theta_{m1}\frac{\partial\chi_0}{\partial\tau}, \tag{16}$$

$$\frac{\partial}{\partial z}\left(\frac{1}{\Pi(\chi_0)}\frac{\partial w_{m1}}{\partial z}\right)+\frac{1}{\Pi(\chi_0)}\left(\frac{\partial^2}{\partial x^2}+\frac{\partial^2}{\partial y^2}\right)w_{m1}=-\left(\frac{\partial^2}{\partial x^2}+\frac{\partial^2}{\partial y^2}\right)\theta_{m1}, \tag{17}$$

where w is the vertical velocity disturbance, and x and y are the horizontal coordinates. The temperature disturbances θ_{m1} have the scale of $\Delta T\,\mathrm{Da}/R_m$ ($=\kappa\nu\Gamma/(g\beta_m L^3)$). The perturbed quantities w_{m1} and χ_1 have the scale of $\Pi_r\kappa/L^3$ and $\kappa\nu/(g\beta_m\Delta C L^3)$, respectively.

The disturbances are expressed in form of periodic waves under the normal mode analysis:

$$[\theta_{m1}, w_{m1}, \chi_1]=[\theta^*_{m1}, w^*_{m1}, \chi^*_1]\exp[i(a_x x+a_y y)] \tag{18}$$

where i is the imaginary number and $a=(a_x^2+a_y^2)^{1/2}$ is the horizontal wave number. An appropriate length scale for the convection in the mushy layer is its thickness H. We rescale the vertical length with the thickness of the mushy layer h ($=2\lambda\tau^{1/2}$). At the onset of convection the amplitude functions of disturbances are assumed to have the following form:

$$[\theta^*_{m1}(\tau,z), w^*_{m1}(\tau,z), \chi^*_1(\tau,z)]=[\theta^*_m(\zeta), w^*_m(\zeta), \chi^*(\zeta)], \tag{19}$$

where $\zeta=z/h(\tau)$ is a similarity variable.

In the liquid layer the vertical velocity disturbance is rescaled with a time-dependent scale factor $h^2(=4\lambda\tau^2)$ based on propagation theory [20]. The perturbation equations in the liquid and mushy layers are transformed by using self-similarity. The self-similar stability equations for the liquid and mushy layers are obtained as follows:

(in the liquid layer)

$$(\overline{D}^2+2\lambda^2\zeta\overline{D}-a^{*2})\theta^*=\frac{R_m^*}{Da^*}w^*\overline{D}\theta_0, \tag{20}$$

$$\left[(\overline{D}^2-a^{*2})^2+\frac{2\lambda^2}{Pr}(\zeta\overline{D}^3-a^{*2}\zeta\overline{D}+2a^{*2})\right]w^*=0, \tag{21}$$

(in the mushy layer)

$$(\overline{D}^2+2\lambda^2\zeta\overline{D}-a^{*2})\theta_m^*=R_m^*w_m^*\overline{D}\theta_{m0}-2\lambda^2St\zeta\overline{D}\chi^*, \tag{22}$$

$$2\lambda^2\zeta[\chi^*\overline{D}\theta_{m0}+\chi_0\overline{D}\theta_m^*+(\theta_{m0}-\gamma)\overline{D}\chi^*+\theta_m^*\overline{D}\chi_0]$$
$$=R_m^*w_m^*\overline{D}\theta_{m0}, \tag{23}$$

$$\left[\overline{D}^2-\frac{\Pi'(\chi_0)}{\Pi(\chi_0)}\frac{\chi_0}{\gamma-\theta_{m0}}\overline{D}\theta_{m0}\overline{D}-a^{*2}\right]w_m^*=a^{*2}\Pi(\chi_0)\theta_m^*, \tag{24}$$

where $'$ represents the derivative $d/d\chi_0$, $\overline{D}=d/d\zeta$, $a^*=ah$, $Da^*=Da/h^2$, and $R_m^*=R_mh$. In the liquid layer, the amplitude of temperature disturbance θ^* has the scale of $\Delta T\, Da/R_m$ $(=\kappa\nu\Gamma/(g\beta_mL^3))$, and the amplitude of vertical velocity disturbance w^* has the scale of $H^2\kappa/L^3$.

The boundary conditions are given by

$$\theta^*=0,\ w^*=0,\ \overline{D}w^*=0 \qquad \text{for } \zeta\to\infty, \tag{25}$$

$$\theta^*=\theta_m^*,\ \overline{D}\theta^*=\overline{D}\theta_m^*-\frac{2\lambda^2St}{\gamma}\overline{D}\theta_0h^* \qquad \text{at } \zeta=1, \tag{26a,b}$$

$$w^*=w_m^*Da^*,\ \overline{D}w^*=0,\ \chi^*=-\frac{\overline{D}\theta_{m0}}{\gamma}h^*\frac{R_m^*}{Da^*} \qquad \text{at } \zeta=1, \tag{26c,d,e}$$

$$\overline{D}w_m^*=-\Pi(1)\left[\overline{D}^3w^*-3a^{*2}\overline{D}w^*-\frac{2\lambda^2}{Pr}(\overline{D}w^*-\overline{D}^2w^*)\right] \qquad \text{at } \zeta=1, \tag{26f}$$

$$\theta_m^*=0,\ w_m^*=0 \qquad \text{at } \zeta=0, \tag{27}$$

where h^* $(=-Da^*\theta_m^*/(R_m^*\overline{D}\theta_{m0}))$ denotes the amplitude function of the disturbance of the liquid-mush interface position. When the reference permeability is chosen as $\Pi_r=\Pi_*(\overline{\chi_0})$, the Darcy-Rayleigh number is defined as

$$R^*=\frac{g\beta_m\Delta C\Pi_*(\overline{\chi_0})H}{\kappa\nu}, \tag{28}$$

$$\overline{\chi_0}=\int_0^1\chi_0(\zeta)d\zeta, \tag{29}$$

where $\overline{\chi_0}$ is the mean porosity of the mushy layer. When the reference permeability is chosen as the permeability at the liquid-mush interface $\Pi_*(1)$, the Darcy-Rayleigh number is defined as $R_1^*=g\beta_m\Delta C\Pi_*(1)H/\kappa\nu$. For a given St, γ, Pr, θ_∞, and Da^*, the minimum value of R^* (R_c^*) and its corresponding value of a^* (a_c^*) are found numerically by employing a shooting method [20]. The R_c^*- and a_c^*-values determine the critical conditions for the onset of convection.

RESULTS AND DISCUSSION

The permeability of the mushy layer is dependent upon its porosity and internal structure. The porosity in the vicinity of the liquid-mush interface, where the dendritic crystals are sparse, is larger than that of the lower region of the mushy layer. The permeability increases with increasing the local porosity χ of the mushy layer. In the present study the mushy-layer-mode instability is studied using the non-uniform permeability model $\Pi(\chi)\propto\chi^3$ considered by previous investigators [7,8,11,14,27]. The model $\Pi(\chi)\propto\chi^3$, in which the permeability is assumed to be finite when the porosity is 1, is a simple form of the Kozeny equation with the specific surface area of the phase boundaries per unit volume of the porous medium considered constant [7] and is appropriate for the Darcy's equation. In the previous study [20] a uniform permeability (Π=1) was considered in the mushy layer during solidification of aqueous ammonium chloride solution.

The dimensionless parameters are set $Da^*=10^{-5}$ and Pr=10, which are appropriate for aqueous solutions. The critical conditions are plotted for St=1 and θ_∞=0.5 with varying the concentration ratio γ in Figs. 2 and 3, and compared with the result of the uniform permeability model Π=1. The dashed curve (----) indicates the model Π=1 and in this case $R_{1,c}^*$ is identical to R_c^*. In Fig. 1(a) the Darcy-Rayleigh number $R_{1,c}^*$ defined in terms of the permeability $\Pi_*(1)$ at the liquid-mush interface is larger than $R_{1,c}^*$ from the model Π=1. A similar trend is reported in the results of Bhatta et al. [27], in which the steady solidification of the mushy layer with an impermeable

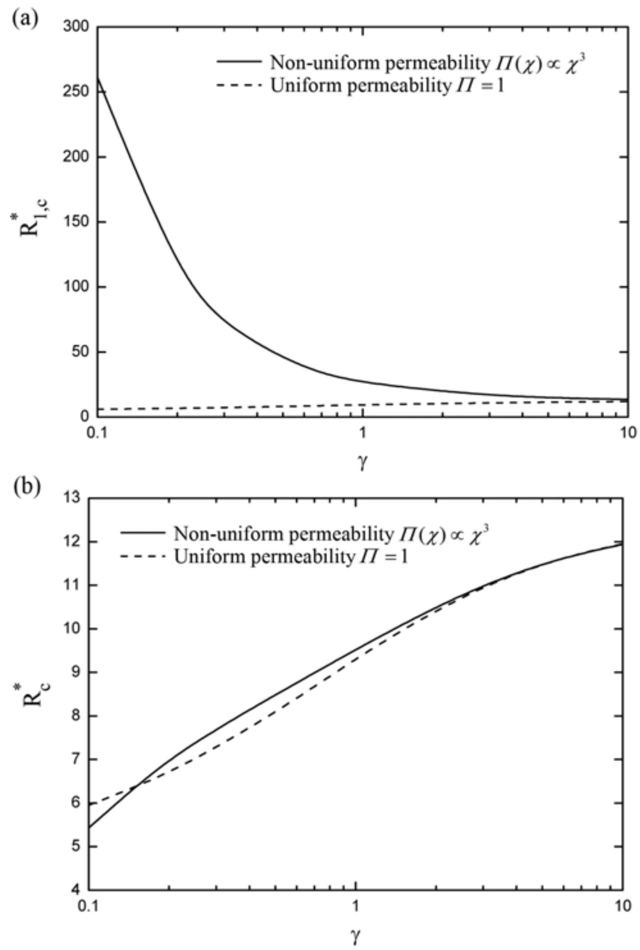

Fig. 2. The variation of the critical Darcy-Rayleigh number with γ for St=1 and θ_∞=0.5. (a) $R_{1,c}^*$ is defined in terms of the permeability $\Pi_*(1)$ at the liquid-mush interface. (b) R_c^* is defined in terms of the mean permeability $\Pi_*(\overline{\chi_0})$. The dashed curve (----) indicates the uniform permeability model Π=1 ($R_{1,c}^*=R_c^*$).

liquid-mush interface is considered. Fig. 2 shows that $R^*_{1,c}$ decreases with γ and the mushy layer is destabilized by increasing γ. R^*_c defined in terms of the mean permeability $\Pi_*(\overline{\chi_0})$ increases with γ, and these trends are consistent with Worster [7]. The difference of

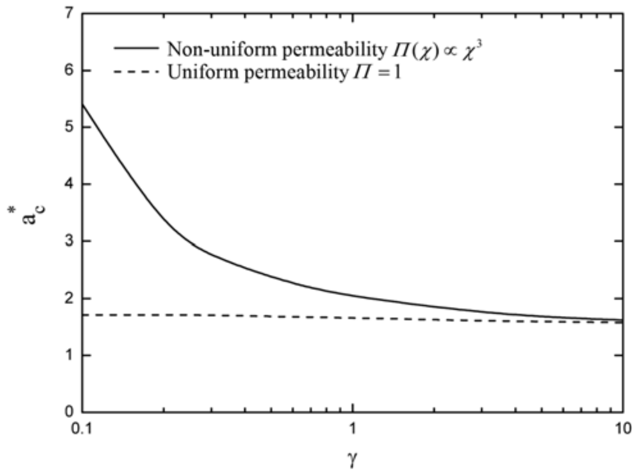

Fig. 3. The variation of the critical wave number a^*_c with γ for St=1 and θ_∞=0.5. The dashed curve (----) indicates a^*_c predicted from the uniform permeability model Π=1.

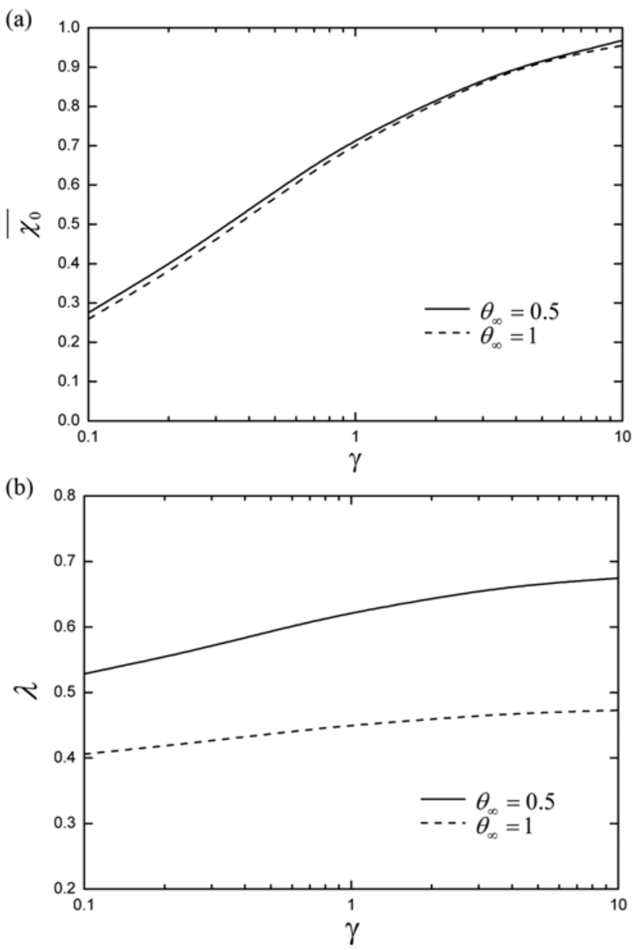

Fig. 4. The variations of (a) the mean porosity $\overline{\chi_0}$ and (b) the phase-change rate λ with γ for St=1.

R^*_c between the non-uniform permeability model $\Pi(\chi)\propto\chi^3$ and the uniform permeability model Π=1 is small for $\gamma\geq1$ and negligible for $\gamma\geq3$, as shown in Fig. 2(b), since the porosity of the mushy layer approaches 1 for a larger γ. The difference of the critical wave numbers a^*_c between the two models is much for a small γ, as shown in Fig. 3.

With increasing γ, the mean porosity of the mushy layer $\overline{\chi_0}$ and the phase-change rate λ increase, as shown in Fig. 4. And $\overline{\chi_0}$ and λ increase with increasing θ_∞, but the influence of θ_∞ on $\overline{\chi_0}$ is weak. When the concentration ratio γ is large ($\gamma\geq10$), the mean porosity is large ($\overline{\chi_0}\geq0.96$) and the permeability variation across the mushy layer is small. Therefore, for a large γ the difference of the critical values between the two models is very small.

When γ is small, the wave number is large and the convective cell is small. The porosity function χ_0 in the mushy layer is given by $\chi_0=\gamma/(\gamma-\theta_{m0})$. For γ=1, St=1 and θ_∞=0.5, the porosity of the mushy layer ranges from 0.5 to 1, and for γ=0.1, the porosity is small in the lower region of the mushy layer and ranges from 0.09 to 1, as shown in Fig. 5(a). For St=1 and θ_∞=0.5, the normalized distributions of velocity disturbances at the critical conditions are shown in Fig. 5(b). The velocity disturbances are more confined to the upper region of the mushy layer for γ=0.1 than for γ=1. When

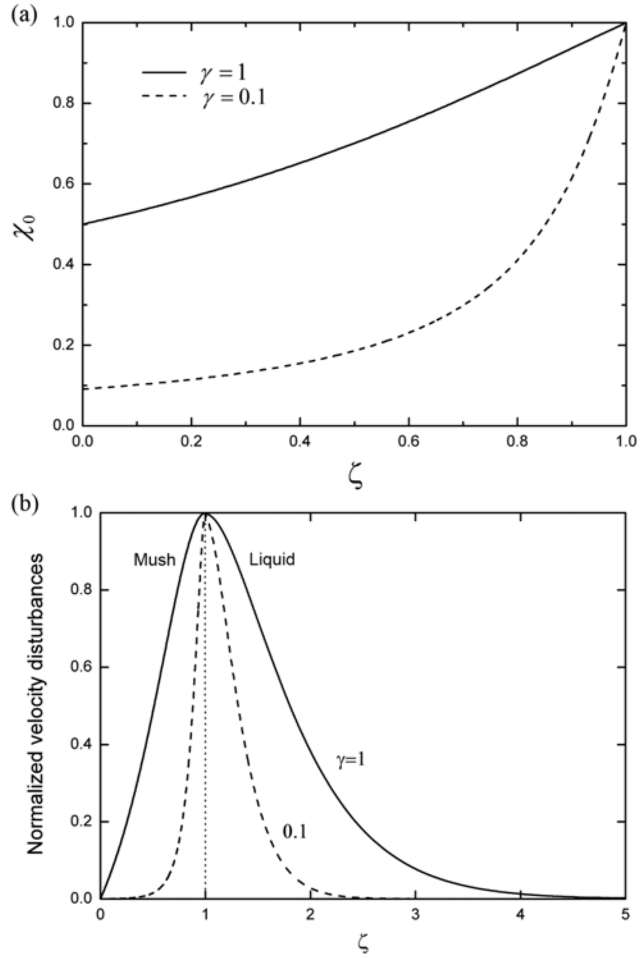

Fig. 5. (a) The profiles of the porosity χ_0 in the mushy layer for St=1 and θ_∞=0.5. (b) The distributions of the normalized velocity disturbances for St=1 and θ_∞=0.5.

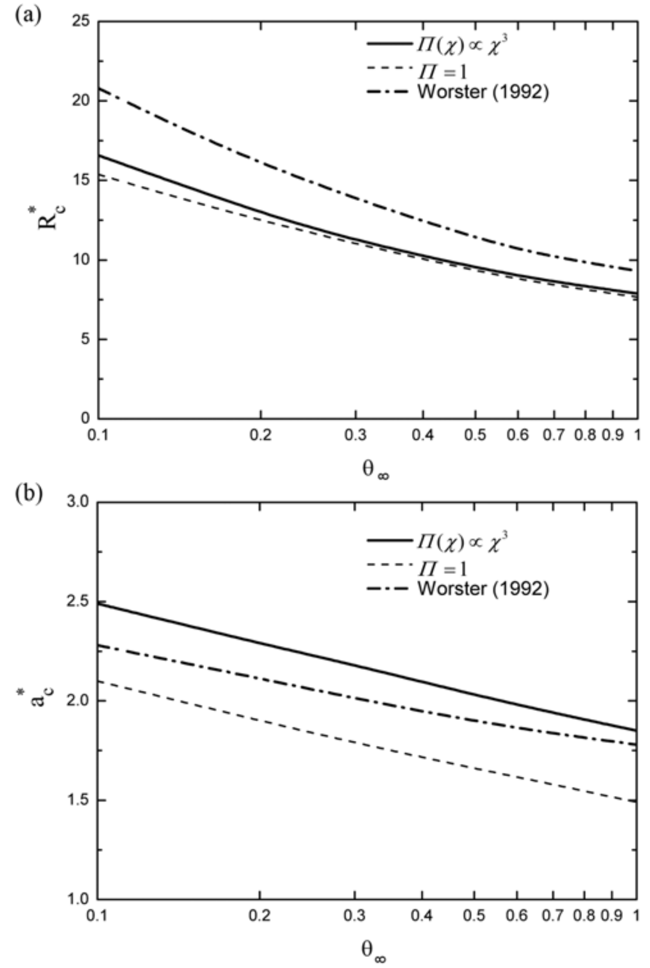

Fig. 6. The variations of (a) the critical Darcy-Rayleigh number R_c^* and (b) the critical wave number a_c^* with θ_∞ for St=1 and γ=1. The present predictions ($\Pi(\chi)\propto\chi^3$ and Π=1) are compared with Worster's [7] results for the steady-state solidification of the mushy layer.

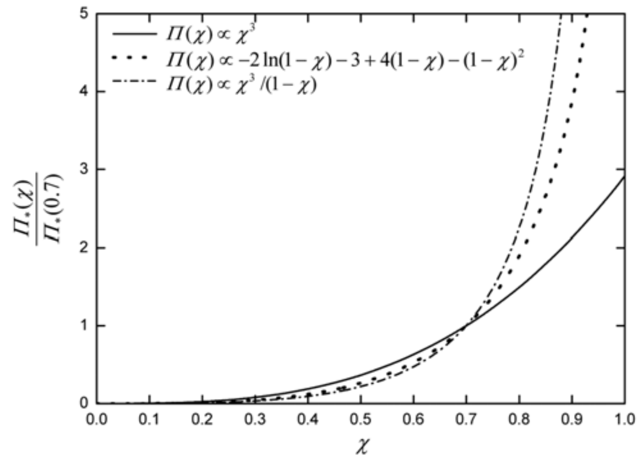

Fig. 7. The variations of the dimensionless permeability functions ($\Pi_*(\chi)/\Pi_*(\bar{\chi})$), scaled by the mean permeability for $\bar{\chi}$=0.7, with porosity χ. The solid curve (—) indicates the permeability model $\Pi(\chi)\propto\chi^3$, the dotted one (·····) indicates $\Pi(\chi)\propto-2\ln(1-\chi)-3+4(1-\chi)-(1-\chi)^2$ in Eq. (31), and the dash-dotted one (-·-·-) indicates $\Pi(\chi)\propto\chi^3/(1-\chi)$ in Eq. (30).

γ is small, the porosity in the lower region of the mushy layer is small and the flow does not penetrate deeply into the mushy layer, resulting in a small convective cell in the vicinity of the liquid-mush interface. These results are supported by Chung and Chen's [15] study, who reported that for a small concentration ratio γ the plume convection occurs at the top of the mushy layer and for a large γ the channel of the plume is generated at the interior of the mushy layer.

In Fig. 6 the critical Darcy-Rayleigh number R_c^* and the critical wave number a_c^* are plotted as a function of the superheat θ_∞ for St=1 and γ=1 and are compared with Worster's [7]. The critical values R_c^* and a_c^* decrease with increasing θ_∞. When θ_∞ is large, the compositional boundary layer thickness in the mushy layer is large and, therefore, the system is more unstable. Worster [7] performed a linear stability analysis for the steady-state solidification of the mushy layer using the model $\Pi=\chi^3$ and obtained the critical Rayleigh number defined in terms of the depth of the mushy layer. The steady basic solution is admitted in Worster's study, while the time-dependent, basic state is considered in the present study. For St=1 and γ=1 the present analysis from the model $\Pi(\chi)\propto\chi^3$ predicts a smaller R_c^* than Worster's, as shown in Fig. 6. The difference between the present R_c^*-values and Worster's increases with decreasing θ_∞, since the growth rate of the mushy layer is high and the time-dependency is strong when the superheat θ_∞ is small.

The permeability for a set of cylinders with parallel flow is modeled as

$$\Pi(\chi)\propto\frac{\chi^3}{(1-\chi)}, \tag{30}$$

which is based on the Kozeny-Carmen equation [12,28]. This function varies considerably near χ=1 and goes to infinity as $\chi\rightarrow1$, while the permeability function $\Pi(\chi)\propto\chi^3$ has a finite value at χ=1. Tait and Jaupart [12] used the following permeability model for the mushy layer:

$$\Pi(\chi)\propto-2\ln(1-\chi)-3+4(1-\chi)-(1-\chi)^2, \tag{31}$$

which was analyzed by Happel and Brenner [29]. Katz and Worster [30] used the model $\Pi(\chi)\propto\chi^2\ln(1-\chi)$, a simplified form of Eq. (31). These functions vary less near χ=1 than the model $\Pi(\chi)\propto\chi^3/(1-\chi)$. Fig. 7 shows the dimensionless permeability functions ($\Pi_*(\chi)/\Pi_*(\bar{\chi})$) scaled by the mean permeability of the mushy layer for $\bar{\chi}$=0.7. The variation of permeability with porosity near χ=1 of the models in Eqs. (30) and (31) is larger than that of the model $\Pi(\chi)\propto\chi^3$. In the present study the permeability is assumed to be finite for χ=1. The permeability functions in Eqs. (30) and (31) are evaluated approximately for $\chi\rightarrow1$ in the present numerical calculation: The functions $\Pi(\chi)$ in Eqs. (30) and (31) are used for $0\le\chi\le0.999$ and the permeability is set to be a constant value of $\Pi(0.999)$ for $\chi>0.999$. The critical values obtained with this approximation are plotted as a function of γ for St=1 and θ_∞=1 in Fig. 8. The models in Eqs. (30) and (31) predict smaller R_c^*-values and larger a_c^*-values than the model $\Pi(\chi)\propto\chi^3$. Therefore, the permeability variation in a mushy layer influences the stability of the compositional convection, and when the variation of permeability is large in the upper region of the mushy layer, the convective cell is small. The differences of R_c^* between the models $\Pi(\chi)\propto\chi^3$ and $\Pi(\chi)\propto-2\ln(1-\chi)-$

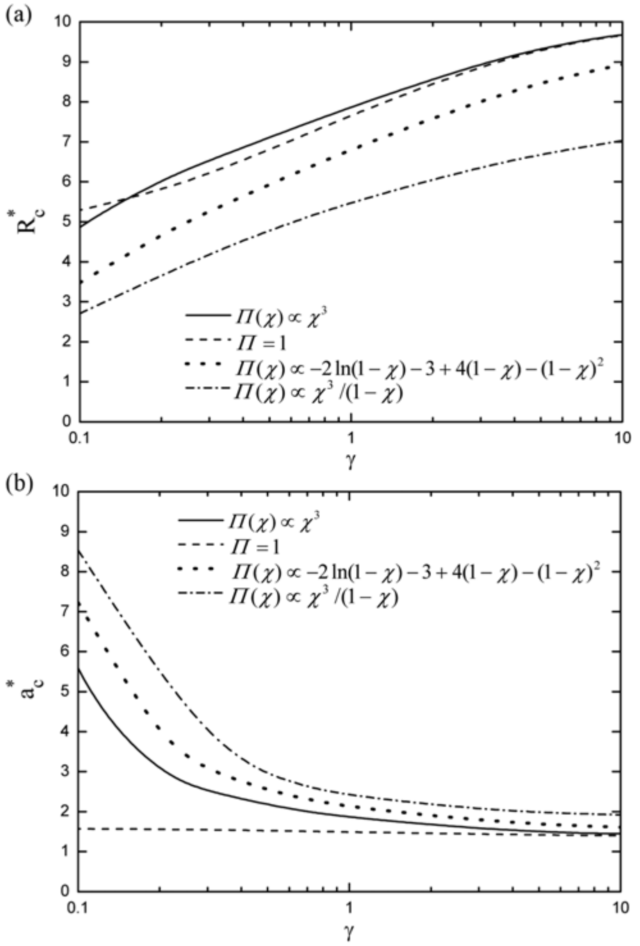

Fig. 8. The variations of (a) the critical Darcy-Rayleigh number R_c^* and (b) the critical wave number a_c^* with γ for St=1 and θ_∞=1. The dotted one (·····) indicates $\Pi(\chi) \propto -2\ln(1-\chi)-3+4(1-\chi)-(1-\chi)^2$ in Eq. (31), and the dash-dotted one (-·-·-) indicates $\Pi(\chi) \propto \chi^3/(1-\chi)$ in Eq. (30).

$3+4(1-\chi)-(1-\chi)^2$ are not much, while the model $\Pi(\chi) \propto \chi^3/(1-\chi)$ predicts smaller R_c^*-values than the other two models.

CONCLUSION

The onset of mushy-layer-mode convection during time-dependent solidification of a binary alloy is investigated implementing linear stability analysis based on propagation theory. The self-similar stability equations for the mushy layer with permeability variation are derived by using the mushy-layer thickness as a length scale. It is found that the critical Darcy-Rayleigh number R_c^*, defined in terms of the mean permeability of the mushy layer, increases with increasing the concentration ratio γ and decreases with increasing the superheat θ_∞, in accord with the previous analysis by Worster [7]. For $\gamma \geq 1$ R_c^*-values from the model $\Pi(\chi) \propto \chi^3$ are close to R_c^*-values from the uniform permeability model Π=1. When γ is small, the mean porosity of the mushy layer is small, leading to small permeability, and small-scale convection appears in the upper region of the mushy layer. The permeability variation in the mushy layer influences the stability of the compositional convection. Various non-uniform permeability models are employed and the results are compared with the case of uniform permeability. When the variation of permeability is large in the upper region of the mushy layer, the critical Darcy-Rayleigh number R_c^* is small with a large wave number. The difference of the critical wave numbers between the non-uniform permeability models and the uniform permeability model is large for a small γ.

REFERENCES

1. C. A. Chung and M. G. Worster, *J. Fluid Mech.*, **455**, 387 (2002).
2. J. G. O'Rourke, A. J. E. Riggs, C. A. Guertler, P. W. Miller, C. M. Padhi, M. M. Popelka, A. J. Wells, A. C. West, J.-Q. Zhong and J. S. Wettlaufer, *Phys. Fluids*, **24**, 103305 (2012).
3. S. H. Whiteoak, H. E. Huppert and M. G. Worster, *J. Cryst. Growth*, **310**, 3545 (2008).
4. P. Guba and M. G. Worster, *J. Fluid Mech.*, **553**, 419 (2006).
5. S. L. Butler, *Phys. Fluids*, **23**, 016602 (2011).
6. A. C. Fowler, *IMA J. Appl. Math.*, **35**, 159 (1985).
7. M. G. Worster, *J. Fluid Mech.*, **237**, 649 (1992).
8. F. Chen, J. W. Lu and T. L. Yang, *J. Fluid Mech.*, **276**, 163 (1994).
9. C. A. Chung and F. Chen, *J. Fluid Mech.*, **412**, 93 (2000).
10. F. Chen, C. A. Chung and M. H. Lai, *Phys. Fluids*, **14**, 1295 (2002).
11. P. W. Emms and A. C. Fowler, *J. Fluid Mech.*, **262**, 111 (1994).
12. S. Tait and C. Jaupart, *J. Geophys. Res.*, **97**, 6735 (1992).
13. D. N. Riahi, *Mechanics Research Communications*, **39**, 18 (2012).
14. G. Amberg and G. M. Homsy, *J. Fluid Mech.*, **252**, 79 (1993).
15. C. A. Chung and F. Chen, *J. Fluid Mech.*, **408**, 53 (2000).
16. A. K. Srivastava and B. S. Bhadauria, *Communications in Nonlinear Science and Numerical Simulation*, **16**, 3548 (2011).
17. D. N. Riahi, *J. Fluid Mech.*, **553**, 389 (2006).
18. S. Govender, *Trans. Porous Media*, **67**, 431 (2007).
19. S. S. L. Peppin, H. E. Huppert and M. G. Worster, *J. Fluid Mech.*, **599**, 465 (2008).
20. I. G. Hwang and C. K. Choi, *J. Cryst. Growth*, **267**, 714 (2004).
21. M. C. Kim and C. K. Choi, *Korean J. Chem. Eng.*, **23**, 874 (2006).
22. M. C. Kim, *Korean J. Chem. Eng.*, **27**, 741 (2010).
23. M. C. Kim, D. Y. Yoon and E. Cho, *Korean J. Chem. Eng.*, **26**, 1461 (2009).
24. I. G. Hwang and C. K. Choi, *Korean J. Chem. Eng.*, **25**, 199 (2008).
25. I. G. Hwang and C. K. Choi, *Korean J. Chem. Eng.*, **26**, 930 (2009).
26. C. K. Choi, J. H. Park, M. C. Kim, J. D. Lee, J. J. Kim and E. J. Davis, *Int. J. Heat Mass Transfer*, **47**, 4377 (2004).
27. D. Bhatta, M. S. Muddamallappa and D. N. Riahi, *Trans. Porous Media*, **82**, 385 (2010).
28. P. Nandapurkar, D. R. Poirier, J. C. Heinrich and S. Felicelli, *Metall. Trans.*, **20 B**, 711 (1989).
29. J. Happel and H. Brenner, *Low reynolds number hydrodynamics*, Martinus Nijhoff Publishers, Dordrecht, Netherlands (1986).
30. R. F. Katz and M. G. Worster, *J. Comput. Phys.*, **227**, 9823 (2008).